Precipitated iron Fischer–Tropsch catalyst manufacturing: impact of Hematite

Dawid J. Duvenhage, Christine Schmidt & Harold W. Wright

Journal of Materials Science
Full Set - Includes `Journal of Materials Science Letters'

ISSN 0022-2461

J Mater Sci
DOI 10.1007/s10853-013-7987-0

Springer

J Mater Sci
DOI 10.1007/s10853-013-7987-0

Precipitated iron Fischer–Tropsch catalyst manufacturing: impact of Hematite

Dawid J. Duvenhage · Christine Schmidt · Harold W. Wright

Received: 10 October 2013 / Accepted: 20 December 2013

Abstract This study found that promoted precipitated iron catalysts, containing large quantities of Hematite, demonstrated adequate activity, selectivity, and attrition resistance operating under commercial Fischer–Tropsch synthesis conditions in a product demonstration slurry bed reactor run over an approximately 170-day period. While small quantities of Hematite (< 10 to about 30 wt %) in the fresh catalyst have been demonstrated to significantly reduce the BET surface area, give rise to catalysts with poor pore structure, and consequently negatively impact the synthesis behavior, it was found that catalytic effective pore volume (> 0.30 cm^3/g) and pore size (60–80 Å) can be induced if larger quantities of about 30–40 wt % Hematite are present in the fresh calcined unreduced catalyst. The catalyst demonstrated exceptional attrition resistance.

Keywords Fischer–Tropsch · Iron catalyst · Supported · Precipitated · Hematite

Introduction/review

The 100 Fe/5 Cu/5 K_2O/25 SiO_2 formulation is probably the most studied commercially viable precipitated iron Fischer–Tropsch catalyst. By the late 1940 s, the catalyst was manufactured as part of the Ruhrchemie–Lurgi Arbeitsgemeinschaft (ARGE) [1] for commercial application. The manufacturing steps as detailed by Frohning et al. [2] is also acknowledged [3] by Sasol Industries in South Africa to mainly represent the precipitated iron catalyst manufacturing procedure for their low-temperature Fischer–Tropsch (LTFT) technology.

Precipitated iron catalysts [2] are essentially prepared from an iron and copper nitrate solution precipitated to a neutral pH with a suitable base, like ammonium hydroxide, sodium hydroxide, and sodium carbonate, using room temperature to near boiling solutions. The freshly formed Ferrihydrite precipitate is filtered to remove the concentrated sodium nitrate containing liquor and then washed with high-purity water to remove the remaining sodium to trace quantities. The washed iron and copper-containing cake is reslurried, promoted (structurally and chemically), and shaped (pelletized or spray-dried depending on the use in fixed bed or slurry bed reactors).

While some reports [2–8] in the open literature generically speak to the importance of precipitation agent concentration, precipitation temperature, and precipitation rate, very few go into detail and none discusses the importance of residence time between preparation steps. For instance, we have found that the residence time between the precipitation step and the filtration step can be critical to obtain a catalyst with performance suitable for commercial use. Ferrihydrite is defined [9] as a "red colloidal gelatinous material, which *is slow to settle and difficult to filter,*" and hence has properties complicating the filtration step where unwanted nitrate-rich liquor is removed from the precipitate. High nitrate content in the catalyst impedes its performance.

Ferrihydrite is described as closely linked polycations consisting of a mixture of "oxo" and "ol" bridging, and its formation is kinetically favored at ambient temperature. In

D. J. Duvenhage (✉) · H. W. Wright
Rentech Inc, 4150 E 60th Ave, Commerce City, CO, USA
e-mail: dduvenhage@rentk.com

H. W. Wright
e-mail: hwright@rentk.com

C. Schmidt
Eltron Research and Development, 4600 Nautilus Court South, Boulder, CO 80301, USA
e-mail: christinems@msn.com

Published online: 14 January 2014

contrast, good catalytic characteristics (surface area, pore volume, and pore size) are benefitted, among others, by elevated precipitation temperature [2–8]. Under rapid elevation of pH, the iron (III) dimer will produce poorly ordered Ferrihydrite. The degree of crystallinity depends on the rate and temperature of the hydrolysis reaction [10–12]. Crystallinity is deemed "undesirable" for optimal catalysis [8]. Well-ordered Ferrihydrite is viewed as a defective Hematite structure of 3.5 nm in diameter [10], while poorly ordered Ferrihydrite, which appears to be amorphous by XRD, consists of spherical particles approximately 2 nm in diameter [13]. These can recrystallize, forming the more ordered six-line XRD Ferrihydrite. At high temperature, this material will transform into Hematite. The small unit cell explains [14] its very poor dewatering ability, hence impacting the rate at which nitrate can be removed from the slurry, and potentially contribute to the formation of Hematite [15].

Pretorius [8] recently concluded that catalysts belonging to the Ferrihydrite family of iron (hydr) oxides, i.e., systems prepared from 2-line Ferrihydrite precursors, and hence only have a small degree of crystallinity, exhibit the "better" Fischer–Tropsch activity when compared to systems prepared from Goethite and organic acid methods. It is stated that Ferrihydrite material *produces catalysts with high surface area and large pore volume, in line with the properties for Hydrous Ferric Oxides* as aforementioned. In mineralogy studies, Schwertmann and Cornell [14] support the low surface area associated with Hematite at 20–90 m^2/g compared to that of Ferrihydrite at 180–200 m^2/g. Elsewhere, surface areas of 320–340 m^2/g are reported for X-ray amorphous iron (hydr) oxide [12, 16] or then Ferrihydrite. This is consistent with the Pretorius report [8]. While the freshly prepared catalyst characteristics do not necessarily indicate expected synthesis behavior, it is important in the sense of quality control during manufacturing of the required product. The fresh catalyst characteristics within a specific catalyst formulation are a pointer toward the comparative reduced catalyst properties.

Attempts in our own laboratory to produce a 100 Fe/5 Cu/5 K_2O/25 SiO_2 acid-to-base precipitated Ruhrchemie-like system resulted in an uncalcined spray-dried BET surface area of 355 m^2/g, 0.55 cm^3/g pore volume, and 63 Å average pore width. This result supports earlier observations [1, 3, 7, 8]. However, the suggestion that ONLY weakly crystalline iron (hydr) oxide materials give GOOD low-temperature Fischer–Tropsch catalysis appears to be in contrast to an observation in US patent 5, 504, 118 by Benham et al. [17], where in the first claim, it reads: "….. iron oxide being selected from the group consisting of hydrous iron oxides, and precipitated iron oxide *comprised predominantly of Hematite*, said activation being effected by ……" This unsupported 79 wt % Hematite containing commercially prepared catalyst (100 Fe/1 Cu/1 K) performed well at above 70 % CO conversion over a 1200-h period in a CSTR and showed good wax-producing behavior (alpha value of ~ 0.95). Little is however reported on this catalytic system, and the observation appears in contrast to the earlier reports [1, 3, 7, 8].

In our own experience, a precipitated iron catalyst scale-up to several 100 kg per preparation is confronted with large liquid volumes of slurry that needs to be transferred quickly and needs efficient filtration to realize Hematite-free catalysts. This typically requires large expensive liquid pump capabilities, large expensive filter presses, and hence the ideal time requirements between process steps are difficult to meet. As already indicated, Ferrihydrite is a difficult-to-filter colloidal gelatinous material and hence difficult to filter, and thus prone to Hematite formation. If the presence of some Hematite may be tolerated in the final catalyst, it implies more flexibility exists between preparation steps at the commercial level, especially when having to remove the unwanted nitrate-rich liquor from the freshly formed precipitate.

This discussion above raises several questions. (1) Does it imply, although iron (hydr) oxide materials appear XRD amorphous, that there are in fact always *smaller than 10 nm crystalline Hematite particles* present that are not detected by XRD? (2) Is there an optimum crystallite size for good precipitated iron catalysts? (3) Can crystallite size be "tailored" during precipitation? (4) Is the presence of "only" small Hematite crystallites below 10 nm important for a good precipitated iron catalyst? (5) Can the presence of significant amounts of Hematite give rise to effective LTFT catalysts? (6) Does the presence of Hematite impact the particle integrity of the catalyst?

While not answering all of these questions, we will demonstrate below that "optimized quantities" of Hematite may be acceptable for low-temperature Fischer–Tropsch (LTFT) precipitated iron catalysts and simplify scale-up requirements as mentioned above. It will be demonstrated how to manipulate Hematite formation in such catalysts during preparation, and to show the significance of optimized quantities of Hematite on particle strength/abrasion resistance, and catalyst activation. It will be demonstrated that while giving rise to "different" surface morphology, when compared to Hematite-free systems, these catalysts still give "effective" low-temperature Fischer–Tropsch (LTFT) performance (activity, time online stability, and selectivity).

Materials and methods

Catalyst preparation

A series of 100 Fe/5 Cu/4.7 K/32 SiO_2 precipitated iron catalysts were prepared by co-precipitation with sodium carbonate at 85 °C and a pH of 8.8. The preparation is

described in detail elsewhere [18]. A reference catalyst was prepared by holding the freshly formed precipitate at the precipitation temperature for an additional 5 min after precipitation before it is filtered. For the purpose of this study, the hold time of the experimental catalysts is varied between 10 and 120 min. After filtration, the sodium-rich cake was washed with room temperature deionized water until free of sodium and nitrates (< 0.50 % sodium) by analyzing the filtrate conductivity down to 30 (± 10) μmho. The washed residue was reslurried, promoted with silica and potassium hydroxide, and spray-dried. The final step involves a multi-step calcination procedure to 500 °C. The final catalyst is classified to between 60 and 80 μm.

Catalyst characterization

Elemental analysis

Inductively coupled plasma analysis (ICP analysis) was performed via standard procedure by Huffman Laboratories, located in Golden, Colorado.

Surface area, pore volume, and pore size

Analysis was performed using a Micromeritics TriStar II instrument. Surface areas and pore sizes were determined from multi-point nitrogen volume/partial pressure isotherms using the BET method. Pore diameters were determined using the BJH desorption method.

X-ray diffraction

X-ray diffraction analysis was carried out using a Siemens Kristalloflex 810 diffractometer using the scan parameters: Range (2θ) 20–70; Step size (2θ) 0.05; Time per step (s) 2.0. The Rietveld refinement method was used for the data analysis through the use of the General Structures Analysis System (GSAS) [19] driven by the graphical user interface EXPGUI [20].

It is important to note that X-ray diffraction will not detect Hematite crystallite entities smaller than 10 nm and hence if present will be excluded from the quantification process. While this potentially may skew the absolute numbers in favor of larger crystallite sizes, the relative comparison between like samples (or samples from the same family) will be valid. A highly crystalline Hematite sample (Aldrich, > wt. 98 %, approximately 5 μm) was used to identify the Hematite XRD diffraction pattern, while the crystallite size was calculated using the full-width half-maximum (FWHM) of the chosen XRD peaks and the Scherrer equation [19]. For the quantification of the Hematite, 10 wt % cesium oxide is mixed into the catalyst sample as an internal standard, which is used to calibrate the scale factor used by the GSAS program to match the program model developed through Rietveld refinement in obtaining experimental data. The scale factor relates the intensity of the experimental data with that of the model. The crystallite size was calculated for four peaks and averaged (the peaks at the 2θ values of 24.1°, 40.8°, 49.4°, and 51.4° were used in this regard).

In the data analysis, instrumental broadening effects were considered and accounted for by instrument calibration using Lanthanum Hexaboride, LaB_6. All peaks associated with Hematite were confirmed with the theoretical peaks produced by PowderCell (a program for the representation and manipulation of crystal structures and calculation of the resulting X-ray powder patterns) [21]. Refinement of the sample shift relative to the diffraction plane (this is an artifact of the way in which the sample was mounted in the diffractometer) was performed and accounted for.

Crystallite size broadening effects were accounted for by the refinement of the profile parameter LX where crystallite size was determined (see modified Scherrer equation below). The unit cell parameters for each phase were refined along with the positional parameters for the iron and oxygen in Hematite. The background was also refined using the power series function type 6 in GSAS with seven terms.

The profile parameter LX, which is synonymous [19, 20] with the Scherrer broadening variable X, is substituted into the modified Scherrer equation below to obtain the apparent particle size in Angstroms. LX describes the Lorentzian profile shape width of a given X-ray diffraction peak and is related to the grain size of a crystalline material by the Scherrer equation.

Instrumental line width also needed to be accounted for. X is equal to the size broadening effects of the sample minus the instrumental line width ($LX_{instrument} = 3.056$). A shape factor K of 4/3 was incorporated into the Scherrer equation as is appropriate for spherical and/or ellipsoidal particles [22]. The particle size in nanometers is obtained by the division of apparent particle size by a factor of ten.

Modified Scherrer equation

$$p = \frac{18000K\lambda}{\pi X} = \frac{18000(4)\lambda}{3\pi X}$$

where K = Scherrer constant at 4/3 due to Ferrihydrite's spherical morphology [22]; λ = X-ray wavelength in Angstroms (Cu in this case = 1.5408 Å); and $X = (LX_{sample} - LX_{instrument}) = (LX_{sample} - 4.886)$.

Example:

$$p_{Hematite} = \frac{18000(1(4(1.5408)))}{3\pi(26.6 - 4.886)} = 542\,\text{Å}$$

$$\text{Crystallite Size} = \frac{\text{Apparent Size}}{10} = 54\,\text{nm}$$

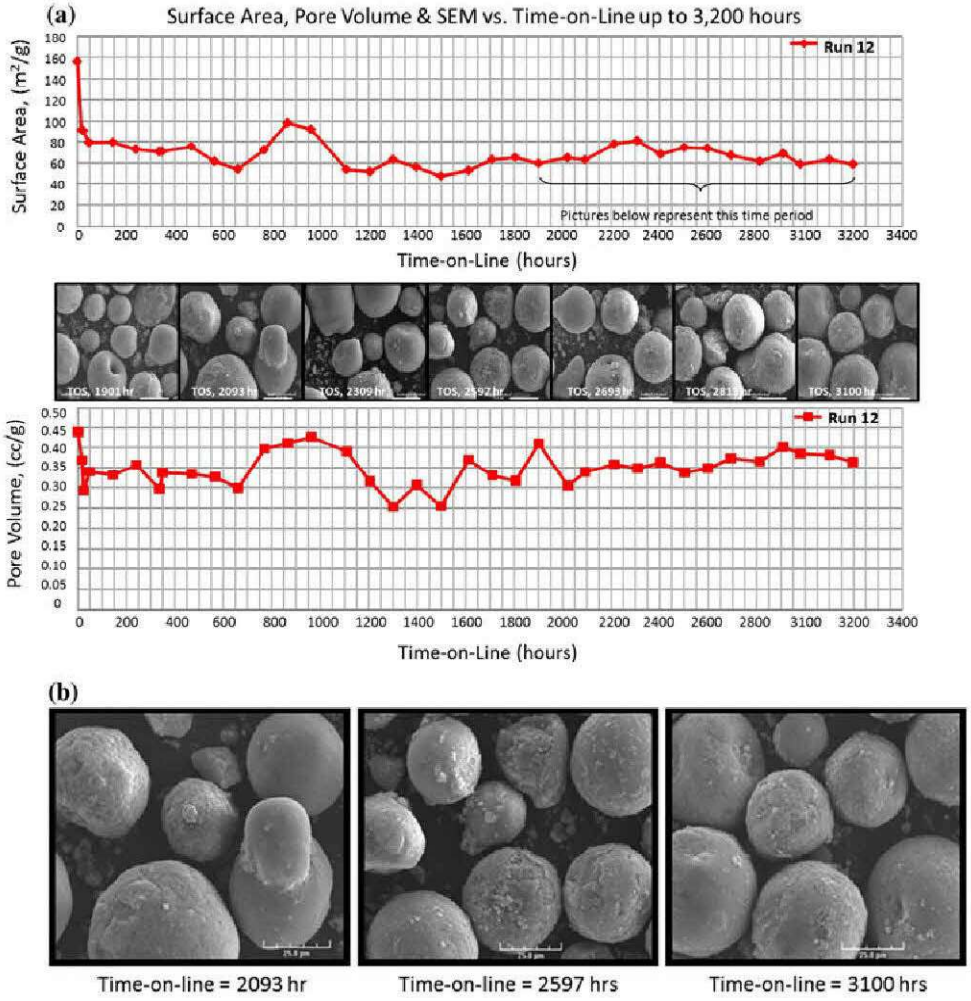

Fig. 1 **a** Run time morphology and surface changes of a precipitated iron catalyst in a 10 barrel-per-day slurry bubble column demonstration unit between 1901 and 3100 h on line (SEM pictures depicted at × 1000 magnification, and the *white bar* to the *bottom right* in each picture represents approximately 25 μm). **b** Run time morphology at × 1000 magnification of three time periods (2093, 2597, and 3100 h) as depicted in Figure a (*white bar* at *bottom right* represents 25 μm)

Temperature-programmed reduction (TPR)

A 22- to 27-mg sample was weighed out and placed within the sample tube on top of a quartz frit of a Micromeritics ChemiSorb 2750. The sample was degassed at 110 °C under a 50 mL/min flow of nitrogen for 1 h and allowed to cool under that same atmosphere prior to testing. Once the sample had cooled, the nitrogen gas was turned off and the testing gas (10 % H_2 in Argon) was turned on and allowed to flow over the sample for 10 min at 50 mL/min prior to testing.

Attrition test

The air jet attrition test was used as an accelerated test to assess relative attrition of 15 g of catalyst and is described in more detail elsewhere [23]. The percent loss of fines after a specified time of treatment gives a measurement of the attrition resistance for the catalyst. The weight of the fines generated at 6 time intervals over a 5-h period was measured, and the relative attrition index was calculated from the slope of the data.

Reactor testing of catalyst

Approximately 10 g of catalyst and about 310 g of C-30 hydrocarbon were loaded into a 2-l laboratory CSTR reactor. The catalyst was activated at 280 °C for 10 h in a mixture of 34 % CO, 54 % H_2, and 12 % N_2 at a SV of about 3.0 Nl_{tot}/g_{cat} and pressure of 140 psig. After the hold time was completed, the reactor was cooled down and the reactor conditions set to 240 °C, 350 psig, 1.6 H_2/CO, and 4.0 Nl_{tot}/g_{cat}.

Results

Catalyst preparation and characterization

ICP characterization confirmed that the approximate catalyst composition as prepared is similar to the target

Table 1 Impact of hold time after precipitation on surface area, pore volume, pore size, Hematite content, attrition index, and temperature-programmed reduction (TPR) peak for calcined reference and test precipitated iron catalysts

Sample #	RI-CS-S-043	RI-CS-S-057	RI-CS-S-058	RI-CS-S-059	RI-CS-S-060	RI-CS-S-067	RI-CS-S-068	RI-CS-S-065
Hold time (min)	5	15	30	45	60	75	90	120
BET surface area (m^2/g)	289	285	277	270	255	263	253	237
Pore volume (PV) (cm^3/g)	0.58	0.45	0.46	0.42	0.38	0.51	0.54	0.52
Ave pore width (PW) (Å)	80	62	66	62	54	77	86	89
PW/PV ratio	138	138	143	148	142	151	159	171
Hematite (wt %)	0.72 (± 0.45)	1.6 (± 0.63)	15.7 (± 2.8)	20.6 (± 0.94)	37 (= 3.4)	51.8 (± 1.8)	50.9 (± 1.6)	49 (± 1.3)
Hematite crystallite size (nm)	Not detectable	Not detectable	17 (± 4)	20 (± 2)	13 (= 2)	18 (± 0.7)	19 (± 0.6)	16 (± 0.4)
Attrition index	~	0.337	0.216	0.231	0.275	0.243	0.213	0.116
1st TPR Peak (°C)	246	244	251	245	237	231	230	209

composition at 100 Fe/5 Cu/4.7 K/32 SiO_2. The sodium content at 0.31–0.40 wt % is slightly better than the expected 0.50 wt % value (Fig. 1).

The surface characteristics of the various calcined catalysts are reported in Table 1.

The Hematite weight percent increased as the hold time increased after precipitation before the filtration step. It is evident from Table 1 and Fig. 2 that the Hematite content increases from nearly nothing (0.7 wt %) for a 5-min hold time up to about 52 wt % after a 75-min hold time.

In all cases, the catalysts yield high surface areas between 237 and 289 m^2/g. There is however a 20 % near linear loss of surface area as the Hematite content increases from about 0.7 wt % up to about 52 wt %. Similarly, there appears to be a near parabolic decrease in pore volume from 0.58 cm^3/g down to about 0.35 cm^3/g at 20 wt % Hematite. At higher Hematite content, the pore structure improves again to ca. 0.50 cm^3/g (it is mentioned in the introduction that typical values are in the order of 0.50–0.70 cm^3/g). The pore width follows a similar, but weaker parabolic trend. It is also observed that there is a near linear increase in the pore width to pore volume ratio. While the significance of this observation is not clear, it appears the pore width increases in relation to the pore size as the Hematite content increases.

Any trend between Hematite content and Hematite crystallite size beyond 20 wt % Hematite seems unlikely. It is observed that there is a sharp increase in crystallite size between about 1 and 15 wt % Hematite content, where after there is little, if any, change.

There is a strong trend (Fig. 3) of improved catalyst reducibility with an increase in Hematite content beyond 20 wt % as analyzed by temperature-programmed reduction (TPR). This is an unexpected observation as Hematite is reported to reduce to Magnetite at temperatures higher than 570 °C [24].

Finally, there appears (Table 1; Fig. 4) to be a significant improvement in the attrition resistance of the catalysts with increasing Hematite content.

Synthesis evaluation

To evaluate the impact of the initial fresh Hematite content in the catalyst on the slurry bed Fischer–Tropsch performance, catalysts with 45-, 60-, 75-, 90-, and 120-min hold times after precipitation were evaluated in a laboratory continuous stirred tank reactor (CSTR). The performance is compared to that of the baseline catalyst (5-min hold time or 0.7 wt % Hematite system). The conversion results are presented in Fig. 5 and the C_5+ selectivity trends in Fig. 6. The baseline catalyst performance at about 600 h is designated as the comparison point, i.e., the *y*-axis point designating 1.00 relative unit (designated "ru") activity or selectivity performance. The performance trends for both

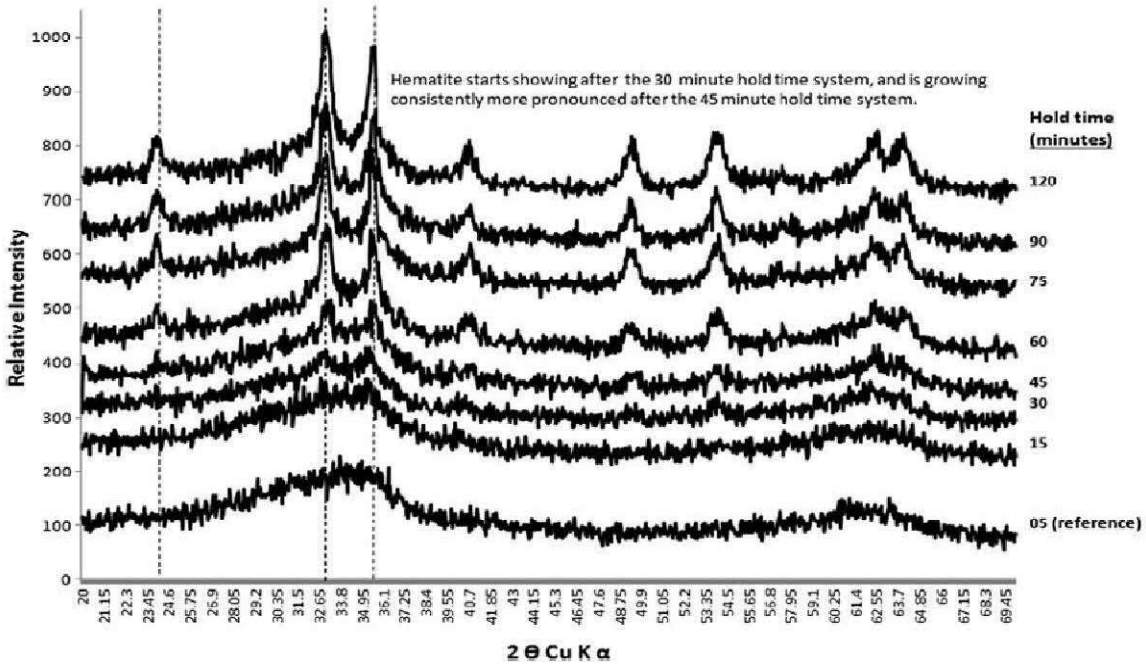

Fig. 2 Impact of increasing hold time after precipitation (5, 15, 30, 45, 60, 75, 90, and 120 min) on Hematite formation as analyzed with X-ray diffraction at approximately 24.05, 32.4, and 35.1 2θ Cu K α

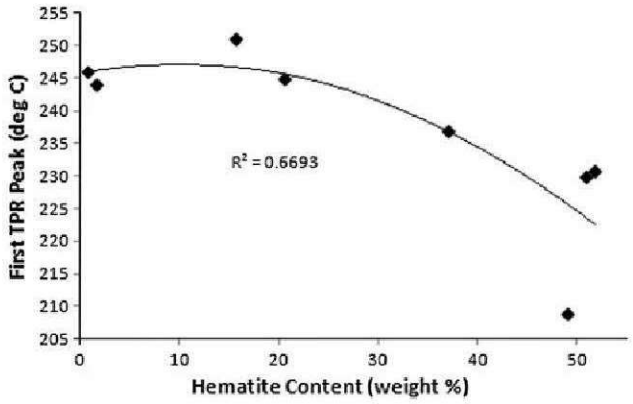

Fig. 3 Impact of increasing Hematite content on the first peak of reduction from a TPR analysis

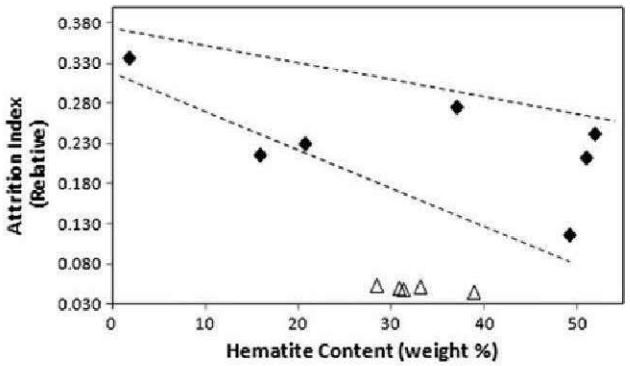

Fig. 4 Impact of increasing Hematite content on the attrition index, and attrition strength of scaled-up (*triangle*) versus laboratory (*diamond*) prepared catalysts (lower index = better attrition)

the baseline and Hematite-containing catalysts are normalized to this point.

The baseline catalyst shows (Fig. 5) an initial decrease in activity and then after about 100 h stabilizes at approximately 1.00 "relative units (ru)" conversion. Surprisingly, after 700 h, the activity of the baseline catalyst slowly starts to increase to a maximum of about 1.2 ru at about 1500 h on line. Thereafter, the conversion slowly decreases over the next 500 h and levels off at about 1.1 ru.

For four of the five Hematite-containing systems (45-, 60-, 75-, and 90-min hold time catalysts), initial conversion begins at approximately the same conversion of 0.88 ru, i.e., nearly 20 % lower than the baseline system. All of these catalysts, except for the 60-min hold time system (37 wt % Hematite), show an activity profile that goes through an initial decrease in conversion before increasing in conversion. The 20 wt % (45-min hold time) Hematite system shows maximum conversion after 500 h on line, which then sharply decreases. The 37 wt % (60-min hold time) Hematite system immediately increases in conversion after activation and sharply climbs to 1.12 ru before it steadily declines, stabilizing after about 1400 h at approximately 1.05 ru. Increasing the Hematite content to 52 wt % (75-min hold time), the system depicts an initial conversion loss over the first 150 h and then sharply increases to about 1.15 ru, only to deactivate at a steady rate dropping down to nearly 0.90 ru after 1400 h on line. The 51 wt % (90-min hold time) Hematite-containing system follows a slightly more delayed decrease in conversion when compared to the 75-min hold time

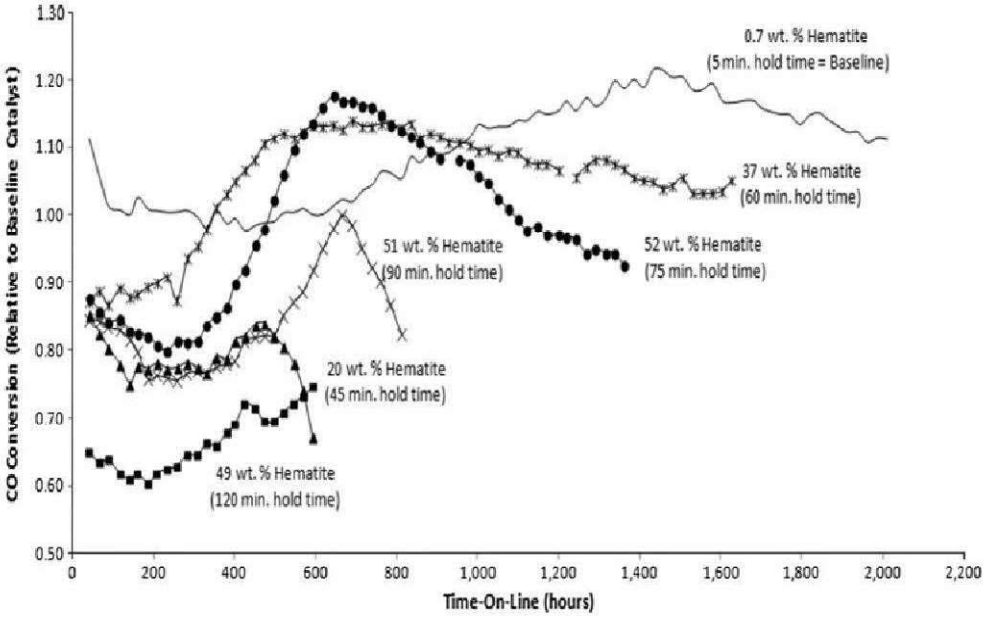

Fig. 5 Impact of increasing Hematite content (*line symbol* 0.7 wt %, *triangle symbol* 20 wt %, *asterisk symbol* 37 wt %, *square symbol* 49 wt %, *times symbol* 51 wt %, and *bullet symbol* 52 wt %) on the relative CO conversion of the catalysts

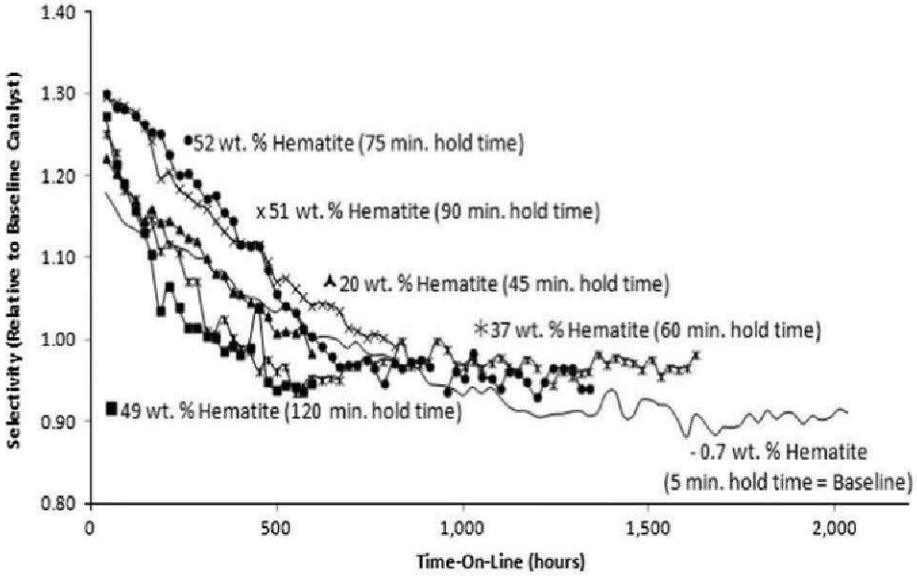

Fig. 6 Impact of increasing Hematite content (*line symbol* 0.7 wt %, *triangle symbol* 20 wt %, *asterisk symbol* 37 wt %, *square symbol* 49 wt %, *times symbol* 51 wt %, and *bullet symbol* 52 wt %) on the relative C_5+ product spectrum

system. On conversion increase, it only gets up to comparative performance for the baseline system after 700 h. The catalyst then shows a rapid decrease in conversion down to about 0.80 ru after approximately 900 h on line. The 49 wt % (120-min hold time) Hematite-containing system depicts poor performance throughout, starting conversion 1.5 ru. After an initial decline of conversion over the first 200 h to 0.60 ru, the conversion slowly increases to about 0.75 ru after nearly 650 h on line. At this point, the run is terminated with the catalyst not achieving full conversion.

The initial C_5+ selectivity of all the Hematite-containing catalysts starts (Fig. 6) at between 1.2 and 1.3 ru, i.e., better than the baseline performance (< 1.2 ru). After about 600 h, the selectivity trends decrease down to 0.95 ru (note that the baseline system starts out slightly lower at just below 1.2 ru its own performance after 600 h and then decreases to about 0.90 ru its initial performance after 1200 h on line). It appears that the 37 wt % (60-min hold time) Hematite-containing system settles at a C_5+ selectivity slightly better (0.98 ru) than the baseline system (0.90 ru). After 1500 h on line, the CO_2 selectivity (not shown) appears to be 1.3 ru after 600 h for both the 37 wt % Hematite and baseline systems. It also appears that the slope for change in CO_2 formation with time (not shown here) is significantly steeper for the Hematite-containing systems than the baseline system. Finally, the methane selectivity (and light hydrocarbon

Table 2 Impact of various freshly precipitated iron slurry filtration and washing sequences on the final Hematite content of the uncalcined catalyst

Catalyst #	Study	Surface area (m^2/g)	Pore volume (cm^3/g)	Pore width (Å)	XRD (wt % Hematite)
RI-CS-S-037-u	No Quench, leave hot hold 3 h at 65 C, wash 65 C	261	0.35	54	34 (± 0.1)
RI-CS-S-038-u	Quenched to 25 C, heat to 65 C, hold 3 h @ 65 C, wash @ 25 C	355	0.35	40	1.3 (± 0.5)
RI-CS-S-039-u	Quenched to 25 C, hold 3 h @ 25 C, wash @25 C	211	0.35	46	1.3 (± 0.6)
RI-CS-S-040-u	Quenched to 25 C, hold 3 h @ 25 C, wash 65 @ C	373	0.40	42	1.7 (+ 0.6)

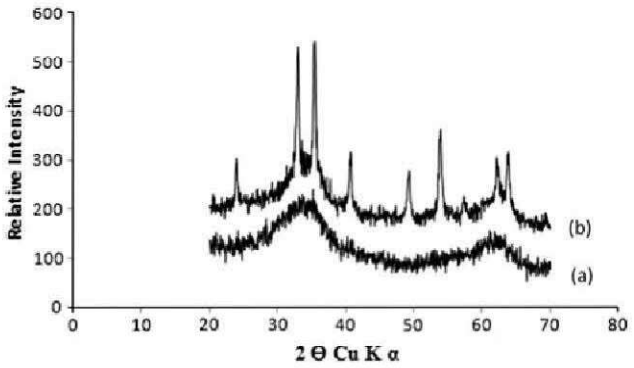

Fig. 7 Uncalcined precipitated iron catalyst from, **a** unaged precipitate showing approximately 0.07 wt % Hematite. **b** Aged precipitate at 65 °C for 3 h showing approximately 34 wt % Hematite

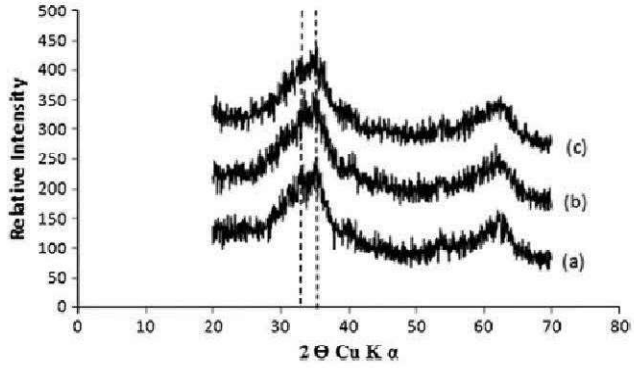

Fig. 8 Uncalcined precipitated iron catalyst from aged precipitate at 65 °C for 3 h. **a** Cold quenched, reheated to 65 °C, held for 3 h, filtered, washed—ambient water. **b** Cold quenched, aged for 3 h at ambient, filtered, washed—ambient water. **c** Cold quenched, aged for 3 h, filtered, washed with 65 °C water

production not shown) depicts variable tendencies with the 45- and 90-min hold time systems following the trend of the baseline system, the 60- and 75-min hold time systems settling in on a trend well below that for the baseline system, and the 120-min hold time system producing a significant amount of light hydrocarbons.

Discussion

Controlling Hematite content in precipitated iron catalyst systems

In the open literature, the topic of Hematite formation in precipitates is mostly confined to the mineralogy sciences [9, 12–14, 16, 24, 25]. Some of these observations however apply to catalyst preparation. Traditionally speaking, precipitated iron catalysts are prepared Hematite-free as the presence of Hematite typically results in inferior catalysis, manifesting a low surface area and poor pore structure development. The question is whether this poor surface morphology is always the rule in the presence of Hematite formation? To evaluate this notion let us first consider how to manipulate and control the level of Hematite in precipitated iron catalysts.

It has been demonstrated in our laboratory that the precalcined precipitated iron catalysts, if prepared free of Hematite until after the washing process, shows great resistance to forming the Hematite phase, even with calcination at high temperature. Catalysts precipitated at 85 °C depict near perfect 2-line Ferrihydrite characteristics, even after calcination at 500 and 600 °C. This is consistent with the literature [3, 19–22]. The surface area of the uncalcined catalyst is high at over 390 m^2/g. Such high surface areas however proved impossible during scale-up.

Catalyst phase information from the impact of catalyst preparation conditions, such as residence time between the precipitation step and filtration step, is limited. There is clear evidence [9] that silica can stabilize the transformation of 2-line Ferrihydrite to Hematite. However, freshly precipitated, silica-free, iron slurries subjected to 65 °C for 180 min (Table 2—RI-CS-S-037-u) before filtration will significantly change the morphology of the catalyst. It contains significant amounts (34 wt %) of Hematite (Fig. 7b) when compared to an ideal Hematite-free system (Table 1—RI-CS-S-043; Fig. 7a). The surface area drops nearly 34 % to 261 m^2/g.

Interestingly, if the freshly precipitated slurry is first rapidly cooled to room temperature with an equal amount of distilled water (cold quenched) and then immediately reheated to 65 °C and held for 3 h, no significant amount of Hematite (1.3 wt %) is formed (Table 2—RI-CS-S-037-u; Fig. 8a). The surface area for this system is only 10 % lower at 355 m^2/g when compared with the baseline system (5-min hold time and no quenching). Two small XRD reflections around 32–35° give an indication of the onset of Hematite formation and probably explain the slightly lower surface area.

Aging a freshly prepared precipitate for 3 h after cold quenching at ambient temperature, and then washing it with room temperature deionized water, gives a similar XRD pattern (see Fig. 8b—1.7 wt % Hematite). However, the measured BET surface area is much lower at 211 m^2/g (Table 2—RI-CS-S-039-u) and could be contributed to the long exposure time to sodium nitrate. Sodium nitrate is an aggressive oxidizer and will rapidly convert iron to rust (i.e., Hematite) [15]. It is thus to be expected that hot iron (oxy) hydroxide precipitates, in the presence of sodium nitrate, will readily transform to Hematite. *A quick filtration step is important if a largely Hematite-free catalyst is to be produced and is thus critical during scale-up*. Our data also show a strong surface area dependence on slurry treatment procedure after precipitation.

These observations furthermore seem to indicate that freshly created hot precipitates are more susceptible to the transformation of the 2-line Ferrihydrite to Hematite, when compared to precipitates "preserved" at ambient temperature. Once the slurry temperature has been cold quenched close to ambient temperature and washed, it appears there is less likelihood that Hematite will form, even after several days. A time delay study between the "wash" and "promotion" steps of adequately washed iron precipitates revealed limited impact on surface area. A filter cake that was promoted and spray-dried 15 days after being filtered and washed showed only a 5 % lower uncalcined surface area at 376 m^2/g when compared to an unaged system at 394 m^2/g.

While it is clear that the phase transformation for quenched precipitates is significantly slower at ambient temperature, it is unclear why the phase transformation is nearly inhibited when the slurry is reheated in the sodium-rich filtrate and left at temperature again. The formation of Hematite at the hot conditions appears to be no surprise as Böhm [25] in 1925 observed freshly precipitated "amorphous Fe(III) hydroxide" rapidly transformed into Goethite if kept for 2 h under 2 M KOH at 150 °C.

In another variation of the cold quench and washing procedure of freshly prepared precipitates, the system is cold quenched, held at room temperature for 180 min, and washed with hot 65 °C deionized water. A near perfect

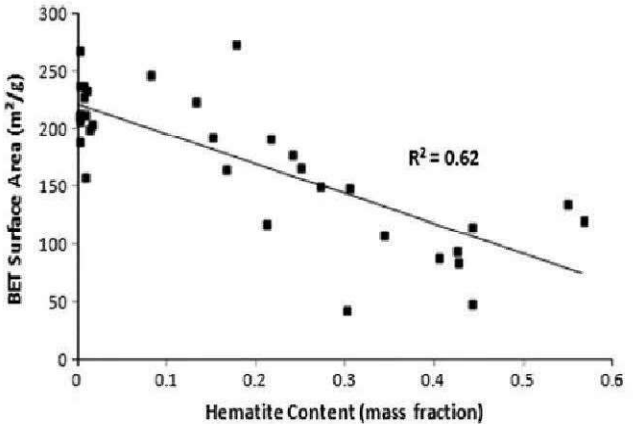

Fig. 9 BET surface area as a function of Hematite content

2-line Ferrihydrite structure was produced as presented by the resulting XRD reflection (Fig. 8c). The surface area is high at 373 m^2/g (Table 2—RI-CS-S-040-u). This procedure does not appear to have a significant impact on the catalyst as the promoted surface area is high, and it cautiously suggests that a "short hot wash" is as beneficial as a "long cold wash." While hot water washes have been supported by pre-1950 s reports [26], it is not clear that wash temperatures as high as 65 °C were used.

A current "lowest Hematite content catalyst" produced in the Rentech laboratory is a system precipitated at 85 °C with a mixture of a ferric nitrate and copper nitrate solutions and a sodium carbonate solution, which is immediately washed with ambient temperature deionized water until free of sodium nitrate (< 0.30 % Na). The resulting catalyst is predominately a 2-line Ferrihydrite, has a high surface area of 420–440 m^2/g, 60 Å average pore width, and pore volumes of 0.64–0.68 cm^3/g. If the catalyst is prepared and washed in a sequence where the fresh precipitate is first cold quenched to ambient temperature, kept at ambient temperature for 3 h, and then washed with ambient deionized water, the surface area drops by 29 % to 313 m^2/g. While the XRD pattern still indicates a predominately 2-line Ferrihydrite structure, *the pore volume is dramatically decreased by about 44 %* (0.66 down to 0.37 cm^3/g), and the average pore width reduces by about 20 % (60 Å down to 48 Å). It is speculated that the cold quench procedure may be inhibiting the removal of residual CO_2 trying to escape from the precipitate, impacting the development of the pore structure, and hence such a methodology to control Hematite content should be avoided.

As earlier suggested, the more crystalline Hematite phase produces poor low surface area LTFT catalysts [8]. Results from the above study in our laboratory indeed suggest (Fig. 9) a strong correlation between BET surface area and the Hematite mass fraction present in the catalyst.

However, it has also been found, as will be shown in the sections below, that if the Hematite content is optimized, the catalyst, contrary to reports mentioned above, preforms comparably to Hematite-free systems.

Hematite-containing catalysts

Catalyst preparation and characterization

Using the concepts discussed in Sect. 4.1.1, a series of catalysts highlighted in the experimental section were precipitated and the fresh slurry kept at the precipitation temperature of 85 °C for 15, 30, 45, 60, 75, and 120 min in the presence of the sodium nitrate-rich filtrate before being filtered and washed with ambient temperature deionized water. These preparations were then compared to a catalyst prepared with the standard preparation hold time of 5 min before the slurry was filtered and washed. These washed Hematite-containing slurries were promoted to contain 4.7 K/100 Fe and 32 SiO_2/100 Fe. The results are presented and discussed below.

It appears that little to no Hematite is present for hold times at 5 and 15 min, but that a very small amount of Hematite started to appear at about 30 min (Fig. 2 with peaks at 24.05, 32.40, and 35.10 2θ). More significantly, there is little difference between the BET surface areas of the calcined catalysts for hold times up to 45 min (Table 1). There is a significant decrease in pore volume and pore size between 5- and 15-min hold times. Experience in our laboratory has taught us that a fresh catalyst with pore volumes and pore size below 0.35 cm^3/g and 50 Å results in poor synthesis performance. It therefore appears while short delay times in slurry treatment after precipitation beyond 5 min and up to 30 min give comparable surface area (285 and 277 vs. 298 m^2/g), the pore volume (0.45 and 0.46 vs. 0.58 cm^3/g) and pore size (62 and 66 vs. 80 Å) were significantly impacted, impeding the catalytic behavior.

The Hematite content correlates well (Table 1; Fig. 2) with slurry hold time at temperature in the presence of the sodium-rich liquor, increasing from 0.7 wt % for a 5-min hold time to about 50 wt % after 75-min hold time, where after it appears to stabilize at this value. There is large scatter in the Hematite crystallite size between 13 and 20 nm for these catalysts (Table 1).

The BET surface area dramatically changes beyond 30-min hold time, dropping to 255–262 and 253 m^2/g, and then 237 m^2/g for 60, 75, 90, and 120 min, respectively (Table 1). Interestingly, while the BET surface area correlates well, linearly decreasing, with increasing Hematite (Fig. 9), the pore volume and pore size appear to follow a parabolic trend initially decreasing only to increase again at longer hold times. The crystallite size appears to stabilize between 16 and 19 nm. Hence, while the pore structure for the intermediate hold times between 15 and 45 min is poor, *the properties significantly improve for hold times between 60 and 120 min. Larger pore widths and pore volumes are evident, giving structures with pore characteristics similar to that of the baseline at 5-min hold time*. This increased hold time of above 60 min may be the critical adaption to the standard practice that allows for adequate residence time during scale-up between the precipitation and filtration steps.

The surface areas of the 60-, 75-, and 90-min hold time calcined catalysts at 255, 263, and 253 m^2/g suggest useful catalysts, especially when considering the pore volumes (0.38, 0.51, and 0.54 cm^3/g) and pore widths (54, 77, and 86 Å). This indicates that catalysts containing enough Hematite may have catalyst properties similar to that of largely Hematite-free systems. This observation was confirmed when a scaled-up version of the 60-min hold time catalyst containing between 28 and 40 % Hematite performed well during a 10 barrel-a-day product demonstration run (PDU run) executed by Rentech in 2012. Such systems appeared to have adequate surface area, acceptable pore volume, and very good pore size.

Further inspection of the laboratory-prepared catalyst results revealed that the presence of Hematite may be benefiting the reducibility of the catalyst, i.e., the more Hematite present, the more reducible the catalyst (Table 1; Fig. 10). The catalyst reduction during TPR analysis showed well-reported [1, 28] three reduction peaks in the order from Hematite (strongly acidic) to Magnetite, Magnetite to Wüstite (weakly acidic), and finally Wüstite to iron metal. As the Hematite content of the catalyst increased, the first TPR reduction peak shifted to lower temperatures. It has been suggested that ferri (oxy) hydroxides are more easily reduced than Hematite [28]. It is thus not exactly clear why the first TPR peak for the higher Hematite-containing systems shifts to a lower temperature. It is postulated that the "finely divided" Ferrihydrite crystallites (< 10 nm, undetected by XRD), typically well dispersed throughout the matrix, has a strong interaction with the support material, which results in the iron phase being reduced at the slightly higher temperature. The increasing quantity of more difficult to reduce larger crystallite size Hematite (15–20 nm) disrupts the strong interaction between the "finely divided" Ferrihydrite crystallites and silica forming a weaker interaction, and improves the reducibility. It may also suggest that there are fewer "finely divided" Ferrihydrite entities present and that a "slightly larger more reducible" crystallites dominate the structure—this is however difficult to verify with the results at hand. Figure 10 includes additional data points for Hematite-containing systems not presented in Table 1 and Fig. 3 highlighting this point. Calcined catalysts with less than 30 wt % Hematite show a first TPR reduction peak between 245 and 251 °C (Table 1). This

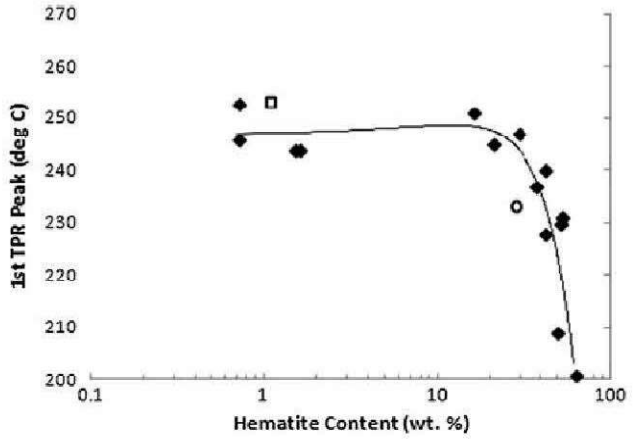

Fig. 10 Impact of increasing Hematite content on the first peak of reduction from a TPR analysis. *Filled diamond symbol* Laboratory-prepared catalysts. *Open square symbol* Hematite-free scaled-up catalyst. *Open circle symbol* Hematite-containing scaled-up catalyst

temperature significantly drops down to about 235 °C at greater than 30 wt % Hematite content. In fact, there appears to be a sharp drop in reduction temperature beyond the 20 wt % Hematite content level. This supports the hypothesis that the formation of Hematite beyond the 20 wt % level gives rise to a more reducible system.

Scale-up (ca. 1000 kg) of a system containing about 40 wt % Hematite displays (Fig. 10) a similar low first TPR peak of about 234 °C compared to that for a scaled-up batch (ca. 1000 kg) containing basically no Hematite at 1.1 wt % giving a first TPR peak of about 252 °C. This may well be "the" reason why the catalyst performed so well during a product demonstration (PDU) run. The reduction peak at about 235 °C is at least 5 °C lower than the PDU run temperature at 240 °C, and this could suggest that the catalyst is "continuously being activated" during the synthesis run. Also interesting is that the data suggested that as the Hematite content increases beyond 40 wt %, the first TPR peak drops sharply from about 234 °C to about 200–210 °C. The much lower reducibility did not result in improved catalysis as will be shown in the section below. It also appears that increasing Hematite content, rather than Hematite crystallite size, is the reason for the improved reducibility of the catalyst, as no definitive correlation with reduction temperature is evident (Table 1).

Importantly, these catalysts seem to have the necessary attrition strength required for stable operation in a slurry bed reactor. In fact, significantly better fresh calcined attrition strength, than obtained in the laboratory, is observed during scale-up of ca. 1000 kg commercial catalyst (Fig. 4). While a fresh calcined catalyst strength does not necessarily implicate activated and run time catalyst strength, the scaled-up catalyst in the aforementioned PDU run passed this test convincingly. The catalyst displayed excellent attrition behavior up to 170 days on line (Fig. 1a, b). The particles stayed larger than 15 μm and were easily separated from the wax product using Rentech's proprietary magnetic settling technology [27].

A final observation (results not shown) is that the freshly spray-dried catalyst appeared to lose less surface area after calcination when containing higher levels of Hematite. This supports the notion of a "stronger" internal core structure for the catalyst. A denser particle is formed, and it is speculated that the particle contracts less on restructuring during calcination and reduction. This is not clear from the packed bed densities at approximately 1.12 versus 0.83 g/ml for scaled-up Hematite-free and 37 wt % containing Hematite systems, respectively. The skeletal densities were similar at 3.8 g/cm^3.

Fischer–Tropsch evaluation

One distinct difference between the "activated" Hematite-containing and baseline catalysts is the longer induction periods (Fig. 5) during the start-up of the CSTR runs. Immediately after activation, the baseline catalyst goes to its "apparent" full conversion (see below). Induction is meant as a post-activation restructuring of the active phase to a catalytic active phase (generally accepted to be iron carbide [1, 3]) to realize maximum "stable" activity. It is well known that a typical iron Fischer–Tropsch catalyst goes through a transformation period during the first 100 h during which iron carbide, the Fischer–Tropsch active phase, is formed [1, 3]. It is not clear that these long induction periods represent periods of carbide formation, but that some form of "slow" restructuring is taking place that gives an improved activity over time. It is apparent from the trends in Fig. 5 that with increasing hold time after catalyst precipitation, this "induction period" becomes longer. The approximate 50 wt % Hematite systems only get to full activity after more than 600 h on line when compared with the 20 and 37 wt % systems, which reach full activity at 440 and 475 h, respectively. Although the Hematite content and crystallite size stabilize at about 50 wt % Hematite content and 16–19 nm Hematite crystallite size after 75-min hold time, the induction period still increases for the catalysts of 75-, 90-, and 120-min hold times. This suggests that a phenomenon other than just Hematite content and Hematite crystallite size is important in these catalysts.

The decreasing lower overall conversion at which the 90- and 120-min hold time systems (both approximately 50 wt % Hematite) stabilize is surprising considering the low first TPR peaks at 230 and 209 °C, respectively. While fresh catalyst surface area is not necessarily an indication of performance, these systems with similar promotion levels have fresh catalyst surface area similar to that of the 60-min hold time system (253 and 237 vs. 255 m^2/g), with

more beneficial pore volume (0.54 and 0.52 vs. 0.38 cm^3/g) and pore size (86 and 89 vs. 54 Å). Even the 75-min hold time system with slightly higher fresh BET surface at 263 m^2/g, 0.51 cm^3/g pore volume, and 77 Å pore size performed poorly. Considering this, it is even further surprising that the 45-min hold time (20 wt % Hematite system) with its much higher surface area (270 m^2/g) and similar surface properties to the 60-min hold time system performed so poorly. Even the first TPR peak is within 4 % at 245 °C compared to 237 °C. Similar behavior translated to two scaled-up catalysts with first TPR peaks at slightly above 250 °C and about 235 °C (Table 1) of which the performance responded accordingly. This seems to suggest that some specific fresh iron phase composition at some reduction temperature lower than 240 °C may be important to obtain adequate catalysis.

The 60-min hold time system at 37 wt % Hematite after a 450-h period reaches full conversion (1.1 ru). Beyond this point, it appears that this Hematite-containing system is out performing the nearly Hematite-free system (Fig. 5) up to about 700 h on line. The presence of the Hematite does not appear to impede the catalyst performance. Then, after nearly 700 h on line, the baseline system starts to increase in conversion, and after nearly 1000 h, its conversion crosses that of the 37 wt % Hematite system. The conversion continuously increases to a maximum at 1.2 tu after about 1500 h on line. The improving conversion after nearly 700 h on line was unexpected, and it is speculated that the activation conditions for this slightly higher silica-containing system (i.e., 32 SiO_2/100 Fe) may not be optimal. It is however clear from this observation that the presence of 37 wt. % Hematite does not have a large negative impact on the activity. In fact, the initial period shows increasing conversion and although the catalyst does not reach the same "high" conversion as the baseline system, the shorter period in which it takes to get to full conversion makes up for that. It is recognized that with an optimized activation procedure and conditions, both these catalysts may perform better.

It is clear from the induction period trends that both the 90- and 120-min hold time catalysts lack the necessary performance to be viable commercial catalysts. What was unexpected was that the latter system, while having similar Hematite content as the 75-min hold time catalyst at about 50 wt %, has a significantly lower first TPR peak at 209 °C compared to 231 °C. This "apparently improved reducibility," having similar crystallite size at 16 and 18 nm, similar pore volume at 0.52 and 0.51 cm^3/g, and pore widths in the same range 89 versus 77 Å, did not translate to similar performance (it is also assumed these systems should restructure similarly on activation). It is furthermore unexpected that the 52 wt % Hematite content for the 75-min hold time system and the 52 wt % of the 90-min hold time system did not show similar performance. The conversion of the latter however is significantly lower when compared to the former (these observations were reproduced). This therefore, considering the 120-min hold time system above, indicates that for longer hold times beyond 60 min, there is another phenomenon that progressively has a larger influence on the performance of these catalysts. To the point where it is very difficult to adequately induce the catalyst after activation, the impact progressively increases to a point where activation itself may become a problem. This may suggest a need for a critical minimum amount of small crystallite size ferri (oxy) hydroxide that is available for "activation" and "induction" to the "more ideal" iron carbide phase.

The 75-min hold time system reached comparable conversion after 650 h to that evident for the 60-min hold time system (Fig. 5). This conversion is nearly 0.2 ru higher than that for the 90-min hold time system. Unfortunately, the catalyst of the 75-min hold time system immediately on reaching its maximum conversion starts to deactivate, and after about 1000 h, the system's CO conversion was already deactivating at 2.3 % per week, compared to only 0.88 % per week for the baseline system. The conversion for the 75-min hold time catalyst appears to begin to stabilize after about 1300 h on line at which point the run was shut down at a conversion of 0.90 ru, deactivating at a rate of 2.0 % per week (Fig. 5). Neither the 90- nor 20-min hold time systems showed adequate run time performance, and the runs were terminated after 600 h on line.

A positive observation is that the Fischer–Tropsch rate of reaction for the baseline and 37 wt % Hematite-containing systems reported here are in the same order of magnitude and at −5.35 mol CO/g cat/s and −5.28 mol CO/g cat/s, respectively, and compares well with values reported by Pretorius [8] at −5.25 mol CO/g cat/s for a "non-crystalline" ferri (oxy) hydroxide-based system. This confirms that "optimized" quantities of Hematite may be beneficial to the performance of the catalyst.

The C_5+ selectivity for all the Hematite catalysts decreased from initially being significantly above that of the Hematite-free baseline system over the first 700 h to a value slightly above after nearly 700 h on line. The selectivity for the Hematite-containing systems appears to be stabilizing at values slightly better than that for the baseline system up to about 1500 h on line (Fig. 6). At low conversion during the induction period, the C_5+ selectivity is high and the CO_2 selectivity low. The decrease in C_5+ selectivity is offset by an increase in CO_2 selectivity as the catalyst becomes more active, produces water, and the water–gas shift reaction becomes stronger with time. Lox et al. [7] demonstrated that iron carbides and iron oxide phases coexist at the time of synthesis and hence

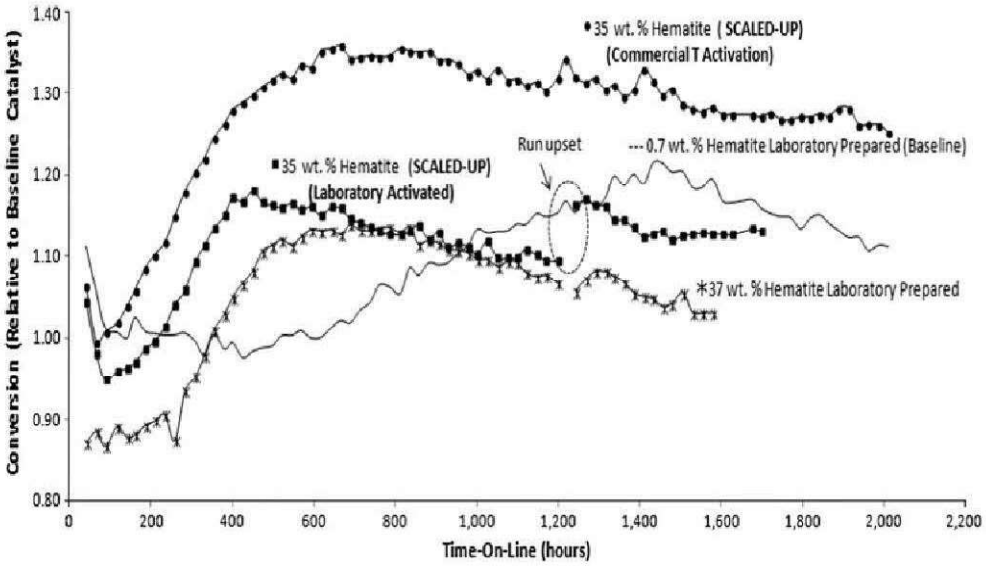

Fig. 11 CSTR performance of scaled-up Hematite-containing catalysts compared to laboratory-prepared catalysts. *Dash symbol* Laboratory-prepared Hematite-free (0.7 wt %) catalyst. *Asterisk symbol* Laboratory-prepared Hematite-containing (37 wt %) catalyst. *Filled square symbol* 2000 lbs scaled-up IIematite-containing (35 wt %) catalyst. *Bullet symbol* 2000 lbs scaled-up Hematite-containing (35 wt %) catalyst at optimized run conditions

would suggest that there is competition for the reactants between the water–gas shift and Fischer–Tropsch reactions. The CO_2 selectivity for our study increases to similar levels for the Hematite-free and Hematite-containing systems. Further interpretation of the selectivity trends may not be useful because of the variation in conversion for these systems.

Scaling up to a 35 (± 3) wt % Hematite content containing catalyst (ca. 1000 kg total batch size) with average Hematite crystallite size of 16 (± 2) Å performed as expected in a laboratory CSTR (Fig. 11). The catalyst performed similarly along a slightly better induction path when compared to the laboratory look a like (37 wt % Hematite content). The laboratory Hematite-free (0.7 wt %) system is also shown for comparison. Upon optimizing the activation conditions, a "plant-activated scaled-up catalyst sample," was transferred from the demonstration activation reactor to a laboratory CSTR under inert atmosphere. The activity profile dramatically improves with the initial conversion increasing to a high, nearly 1.3 relative units. The catalyst stabilizes at a performance nearly 1.8 ru and deactivated at a mere 0.35 % per week. The long induction periods after activation, as experienced during the laboratory studies, did not realize for the Rentech product demonstration run as the catalyst immediately after activation went to full conversion. This catalyst ran for approximately 170 days at good activity, selectivity, and catalyst replacement rate, without any major indication of attrition. It was thus with this run clearly demonstrated that by controlling the residence time between the precipitation and filtration steps during catalyst manufacturing, adequate Hematite content can be induced to give a catalysts with suitable surface characteristics, to be a good commercial Fischer–Tropsch catalyst.

Conclusions

It has been demonstrated that "optimized quantities" of Hematite in precipitated iron catalysts can be useful and give rise to effective LTFT behavior. This result may significantly simplify the scale-up and large scale manufacturing of precipitated iron catalysts because it appears difficult to scale up a Hematite-free catalyst. While having different surface morphology and surface characteristics compared to predominantly Hematite-free catalysts, the presence of Hematite supports better attrition and activation behavior while maintaining "effective" low-temperature Fischer–Tropsch (LTFT) catalysis (activity, time online stability, and selectivity).

It is clearly demonstrated that by manipulating the hold time between the precipitation and filtration steps during catalyst preparation, the Hematite content and crystallite size of the uncalcined catalyst can be varied between 0.5 and 50 wt %. The exposure time of the freshly formed precipitate with the concentrated sodium nitrate solution, a product of the precipitation reaction, at temperature has a significant impact on final catalyst surface area, pore volume, and pore size.

Catalysts containing between 35 and 40 wt % Hematite content demonstrated adequate Fischer–Tropsch activity, selectivity, and attrition behavior during slurry bed operation, and the result could be repeated for a scaled-up version of the catalyst as run in a commercial 10 barrel-a-day product demonstration unit. This benefits manufacturing of the catalyst, as less stringent time requirements are imposed between production steps.

Low quantities of Hematite between about 1.5 wt % to about 25 wt % may well impede performance through a combination of decrease in surface area and poor pore structure development (pore volume and pore size).

Allowing increased amounts of Hematite to form in a controllable manner between 25 and 45 wt % could potentially benefit the pore structure, although at somewhat lower surface area.

An increase in Hematite content appears to coincide with improved reducibility and attrition behavior of the catalyst. However, beyond some point of Hematite formation, or time of sodium nitrate exposure, although the "apparent" reducibility improves, the performance deteriorates.

The basic selectivity and product slate of a run time stabilized Hematite and Hematite-free catalyst appear to be similar.

Acknowledgements We wish to thank Rentech, Inc., for the opportunity to present this work. Acknowledgment also goes out to the contributions of the Rentech support staff. A special word of thanks to Karl Kharas and Braden Peterson for their contributions characterizing and quantifying the Hematite content and crystallite size using XRD. We also appreciate Christa Loux, Mark Still, and Khalid Azzam for their contributions toward catalyst characterization, catalyst activation, and performance testing.

References

1. Steynberg A (2004) Introduction to Fischer–Tropsch technology. In: Steynberg A, Dry ME (eds) Fischer–Tropsch technology. Elsevier, Amsterdam, pp 26–45
2. Frohning CD, Köbel H, Ralek M, Rottig W, Schnur F, Schulz H (1977) The Fischer Tropsch process. In: Falbe J (ed) Chemical feedstocks from coal. Wiley, New York, pp 309–432
3. Dry ME (1981) Technology of the Fischer–Tropsch process. In: Boudart M, Anderson JR (eds) Catalysis-science and technology. Springer, Heidelberg, pp 159–255
4. Espinoza RL, Gibson P, Scholtz JH (2009) USA Patent 7, 547, 657
5. Storch HH, Golumbic N, Anderson RB (1951) The Fischer–Tropsch and related syntheses. Wiley, New York
6. Storch HH, Anderson RB, Fischer LJ, Hawk CO, Anderson HC, Golumbic N (1948) Synthetic liquid hydrocarbon from hydrogenation of carbon monoxide—part 1—review of literature: Bureau of Mines Research on Effect of Catalyst Preparation, Reduction, and Induction Procedures on Activity; Correlation of Physical Properties of the Catalysts with Their Activity, Washington
7. Lox ES, Marin GB, de Graeve E, Bussiere P (1988) Characterization of a promoted precipitated iron catalyst for Fischer–Tropsch synthesis. J Appl Catal A 40:197–218
8. Pretorius PJ (2011) On the preparation of low temperature iron Fischer–Tropsch catalysts: strategies that work and those that do not. In: de Klerk A, King DL (eds) Synthetic liquids production and refining. ACS Publications, Oxford University Press, Inc., Washington, DC, pp 111–125
9. Jamieson EJ (1995) Precipitation and characterization of Iron(III)Oxy hydroxides from acid liquors. PhD Dissertation, Murdoch University, Perth, Western Australia
10. Johnston JH, Lewis DG (1986) A study of the initially-formed hydrolysis species and intermediate polymers and their role in determining the product iron oxides formed in the weathering of iron. In: Long GJ, Stevens JG (eds) Industrial applications of the Mössbauer effect. Plenum Press, New York, pp 565–583
11. Murad E, Johnston JH (1987) Iron oxides and oxyhydroxides. In: Long G (ed) Mössbauer spectroscopy applied to inorganic chemistry. Plenum Press, New York, pp 507–582
12. Cornell RM, Giovanoli R (1989) Effect of cobalt on the formation of crystalline iron oxides from ferrihydrite in alkaline media. J Clays Clay Miner 37(1):65–70
13. Eggleton RA, Fitzpatrick RW (1988) New data and a revised structural model for Ferrihydrite. J Clays Clay Miner 36(2):111–124
14. Schwertmann U, Cornell RM (1991) Iron oxides in the laboratory: preparation and characterization, 2nd edn. WILEY-VCH, Weinheim
15. Kelly J (2004) Gunpowder: alchemy, bombards, & pyrotechnics: the history of the explosive that changed the world. Basic Books, New York
16. Gast RG, Landa ER, Meyer GW (1974) The interaction of water with goethite (–FeOOH) and amorphous hydrated ferric oxide surfaces. J Clays Clay Miner 22:31–39
17. Benham CB, Bohn MS, Yakobson DL (1996) USA Patent 5, 504, 118
18. Duvenhage DJ, Schmidt C, Still M, Azzam K, Kharas K, Hinegnaw S, Ionkina O, Huang R, Wright HA (2013) USA Patent Application 61/764153
19. Larsen AC, Von Dreele RB (2004) General structure analysis system (GSAS), Los Alamos National Laboratory Report LAUR 86-748, pp 1–231
20. Toby BH (2001) EXPGUI, a graphical user interface for GSAS. J Appl Cryst 34:210–213
21. Kraus W, Nolze G (1996) PowderCell—a program for the representation and manipulation of crystal structures and calculation of the resulting X-ray powder patterns. J Appl Cryst 29:301–303
22. Xu Q, Kharas KC, Croley BJ, Datye AK (2011) The sintering of supported Pd automotive catalysts. ChemCatChem 3(6):1004–1014
23. ASTM D 5757 – 11, Standard test method for determination of attrition and abrasion of powdered catalysts by Air Jets
24. Wagner D, Devisme O, Patisson F, Ablitzer D (2006) A laboratory study of the reduction of iron oxides by hydrogen. In: Kongoli F, Reddy RG (eds) Sohn international symposium, San Diego, TMS, vol 2, pp 111–120
25. Böhm J (1925) Über Aluminium- und Eisenoxide I. Z Anorg Chem 149:203–218
26. Hall CC, Craxford SR (1946) Additional information concerning the Fischer–Tropsch process and its products, B.I.O.S. Final Report No. 1722, Item No. 22, British Intelligence Objectives Sub-Committee, pp 110–139
27. Mohedas S, Wright HA (2010) USA Patent Application 20100113622
28. Jozwiak WK, Kaczmarek E, Maniecki TP, Ignaczak W, Maniukiewicz W (2007) Reduction behavior of iron oxides in hydrogen and carbon monoxide atmospheres. J Appl Catal A Gen 326(1):30:17–27